

Polarizations of CMB and the Hubble tension

Noriaki Kitazawa

Department of Physics, Tokyo Metropolitan University,
Hachioji, Tokyo 192-0397, Japan
e-mail: noriaki.kitazawa@tmu.ac.jp

Abstract

Future precision measurements of CMB polarizations can shed new light on the problem so called Hubble tension. The Hubble tension comes from the difference of the evolutions of the Hubble parameter which are determined with two different distance ladders. The standard distance ladder with the observation of Cepheid variables and type Ia supernovae gives larger values of the Hubble constant, and the inverse distance ladder with the observation of the baryon acoustic oscillations both in the CMB and in the clustering of galaxies gives smaller values of the Hubble constant. These different evolutions of the Hubble parameter indicate different evolutions of the free electron density in the process of the reionization of the universe and different magnitudes of low- ℓ polarizations of the CMB, since these polarizations are mainly produced through the Thomson scattering of CMB photons off these free electrons. We investigate the effect on CMB E-mode and B-mode polarizations of $\ell \leq 11$ assuming non-trivially time-dependent equation of state of dark energy. We find that the case of the standard distance ladder gives higher power of polarizations than the prediction in the Λ CDM model.

1 Introduction

The current status of the determination of the Hubble constant, or the present expansion rate of the universe, may indicate the physics beyond the Λ CDM model. The PLANCK collaboration gives a very precise value

$$H_0 = 67.4 \pm 0.5 \quad [\text{km/s Mpc}] \quad (1)$$

from the observation of the CMB assuming the Λ CDM model [1]. On the other hand, a direct measurement with the standard distance ladder using type Ia supernovae with Cepheid variables gives a precise value

$$H_0 = 74.03 \pm 1.42 \quad [\text{km/s Mpc}] \quad (2)$$

without assuming the Λ CDM model [2]. The discrepancy of these two values is beyond 4σ in statistical significance, and in fact they are extremes in many other measurements and determinations. Another direct measurement with the standard distance ladder using type Ia supernovae with the tip of the red giant branch method [3] gives a value $H_0 = 69.6 \pm 0.8 \pm 1.7$ [km/s Mpc] which does not completely agree with the value with Cepheid variables in [2]. The BOSS collaboration gives a value $H_0 = 68.6 \pm 1.1$ [km/s Mpc] from the signatures of Baryon Acoustic Oscillations in redshift-space galaxy surveys assuming the Λ CDM model [5]. This value is obtained with the inverse distance ladder [4] using the determination of sound horizon scale in the CMB assuming Λ CDM model. The value of the obtained Hubble constant is consistent with that of [1].

The SPT collaboration give a value $H_0 = 72.0^{+2.1}_{-2.5}$ [km/s Mpc] from the SPTpol survey for the CMB lensing combined with the signatures of Baryon Acoustic Oscillations in other galaxy surveys assuming the Λ CDM model [6]. This value is not fully consistent with that of [1], though the method is essentially the same, looking different ranges of angular scales of the CMB perturbations. The Megamaser Cosmology Project give a value $H_0 = 73.9 \pm 3.0$ [km/s Mpc] which is independent of the standard and inverse distance ladders [7], though still the error is not small. The measurement using strong gravitational lensing by the H0LiCOW

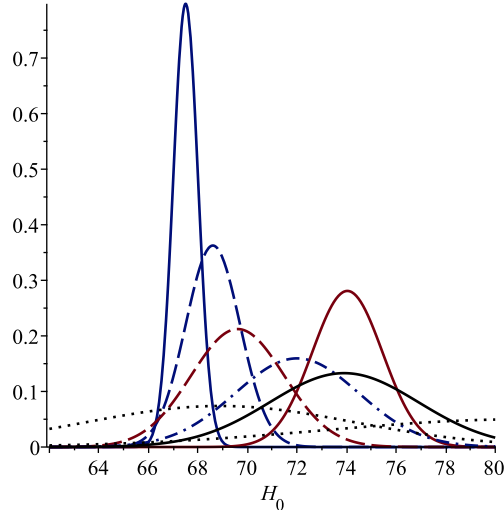


Figure 1: The current status of Hubble constant measurements. Each measurement is shown as a normalized Gaussian distribution with a corresponding error: the solid blue line; the PLANCK collaboration, the dashed blue line; the BOSS collaboration, the dash-dotted line; the SPT collaboration, the solid red line; type Ia Supernovae with Cepheid variables, the dashed red line; type Ia supernovae with the tip of the red giant branch method, the solid black line; the Megamaser Cosmology Project, and the dotted black lines; two extreme results by the H0LiCOW collaboration.

collaboration [8] is also independent of the standard and inverse distance ladders, and they give a value $H_0 = 73.3^{+1.7}_{-1.8}$ [km/s Mpc], but it is the statistical combination of six values of measurements on different quasars distributing a wide range between $H_0 = 81.1^{+8.0}_{-7.1}$ and $H_0 = 68.9^{+5.4}_{-5.1}$ [km/s Mpc], and we need to wait more measurements. These measurements are summarized in Fig.1, and our intension here does not give a complete summary, but gives a simple sketch of current status. This situation so called Hubble tension could merely happen as statistical fluctuations or by some systematic errors, but it might suggest something worth to investigate.

Since there is a tendency that the lower redshift measurements give larger values of the Hubble constant, we may consider only the lower redshift physics not to disturb the success of the Λ CDM model for higher redshift physics, as it has been extensively discussed in [9]. On the other hand, since there could be some internal inconsistencies in the measurements between high and low multipoles and also in the measurements of weak lensing effects by the PLANCK collaboration [1, 10, 11, 12, 13, 14, 15], it may be required more extensive revision of the Λ CDM model (see [16] for a review). In this work we consider the former possibility

and investigate the chance to see some evidences of physics beyond the Λ CDM model in future precise measurements of the low- ℓ polarizations of the CMB by LiteBIRD, for example.

We may consider that the dark energy is not the cosmological constant, but something else which can be captured by considering time-dependent equation of state $p = w\rho$ like

$$w = w_0 + w_a(1 - a) = w_0 + w_a \frac{z}{1 + z}, \quad (3)$$

where and throughout this paper the scale factor is normalized as $a = 1$ at present. This model is called Chevallier-Polarski-Linder (CPL) model [17, 18]. The cosmological constant is represented simply by $w_0 = -1$ and $w_a = 0$. The value of w_0 represents the present value of w and w_a describes a time dependence of the equation of state. The evolution of the Hubble parameter is given as

$$H(z) = H_0 \sqrt{\Omega_m(1+z)^3 + \Omega_{\text{DE}}(1+z)^{3(1+w_0+w_a)} e^{-3w_a \frac{z}{1+z}}}, \quad (4)$$

where we set $\Omega_m = 0.3$ and $\Omega_{\text{DE}} = 1 - \Omega_m = 0.7$ so that it reduces to that of the Λ CDM model in case of $w_0 = -1$ and $w_a = 0$.

We also consider a simple Taylor expansion

$$w = w_0 + w_1 a + \frac{1}{2} w_2 a^2 = w_0 + w_1 \frac{1}{1+z} + \frac{1}{2} w_2 \frac{1}{(1+z)^2} \quad (5)$$

with $w_0 = -1$. The intention is to capture small deviation from the case of the cosmological constant by two parameters, w_1 and w_2 . The amount of the deviation can be larger at recent $a \sim 1$ than at far past $a \sim 0$. The evolution of the Hubble parameter is described as

$$H(z) = H_0 \sqrt{\Omega_m(1+z)^3 + \Omega_{\text{DE}}(1+z)^{3(1+w_0)} e^{3w_1(1-\frac{1}{1+z}) + \frac{3}{4}w_2(1-\frac{1}{(1+z)^2})}} \quad (6)$$

with $w_0 = -1$, $\Omega_m = 0.3$ and $\Omega_{\text{DE}} = 1 - \Omega_m = 0.7$.

We perform two simple fits of H_0 , w_0 and w_a with two sets of data: one is obtained with the standard distance ladder and the other is obtained with the inverse distance ladder. The data

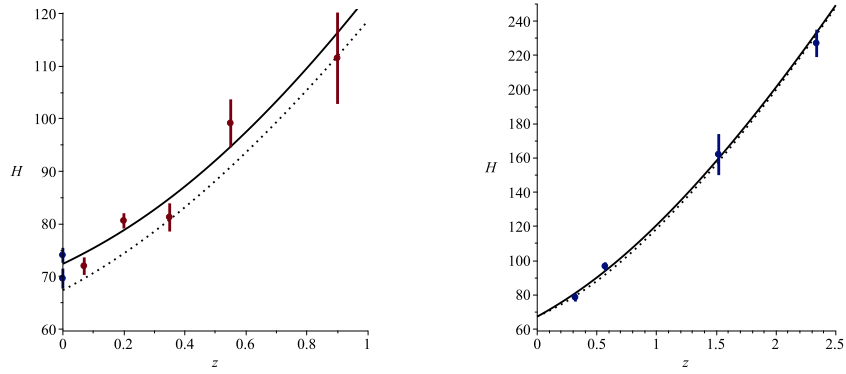


Figure 2: Fits of parameters in the CPL model. The solid lines indicate the results of fits and dotted lines indicate the concordance Λ CDM expectation by the PLANCK collaboration. Left: the fit with the data set of the standard distance ladder which gives $H_0 = 72.4$ [km/s Mpc], $w_0 = -1.06$ and $w_a = -0.34$. Right: the fit with the data set of the inverse distance ladder which gives $H_0 = 67.3$ [km/s Mpc], $w_0 = -0.88$ and $w_a = -0.15$.

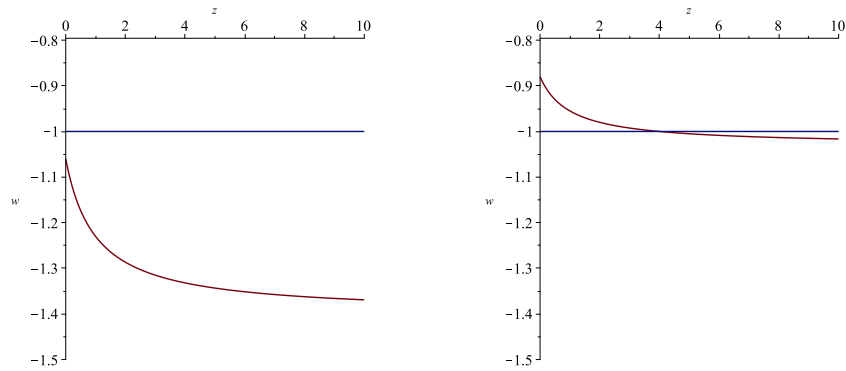


Figure 3: Redshift-dependences of w in the CPL model. Left: the case of the standard distance ladder ($w_0 = -1.06$ and $w_a = -0.34$). Right: the case of the inverse distance ladder ($w_0 = -0.88$ and $w_a = -0.15$).

set of the standard distance ladder consists the values of Hubble parameters in [2] and [3] (they use the same set of type Ia supernovae in the Large Magellanic Cloud with different distance calibration methods) and five determinations of the Hubble parameter at different redshifts using Pantheon + MCT type Ia supernovae in [19]. The data set of the inverse distance ladder consists four values of the Hubble parameter by the BOSS collaboration at different redshifts in [20, 21, 22, 23] and the PLANCK result of the Hubble constant in [1] which we translate to the Hubble parameter at $z = 1000$ assuming the Λ CDM model.

Fig.2 shows the results of our simple least χ^2 fits for the CPL models. The obtained sets of the values of w_0 and w_a for the standard distance ladder and the inverse distance ladder are

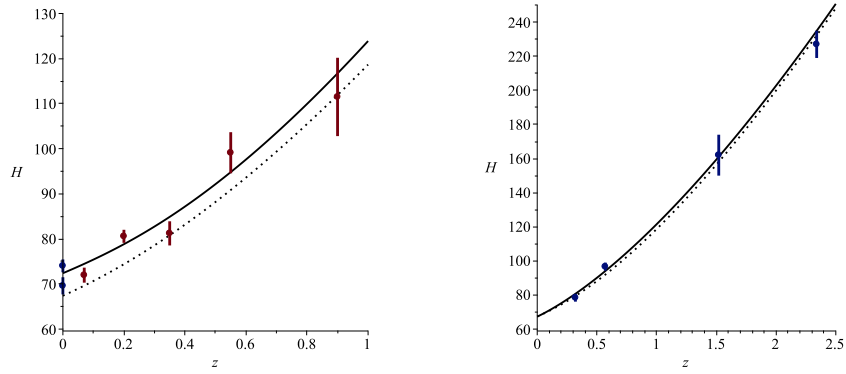


Figure 4: Fits of parameters of the model of Taylor expansion. The solid lines indicate the results of fits and dotted lines indicate the concordance Λ CDM expectation by the PLANCK collaboration. Left: the fit with the data set of the standard distance ladder which gives $H_0 = 72.4$ [km/s Mpc], $w_1 = -0.60$ and $w_2 = 1.1$. Right: the fit with the data set of the inverse distance ladder which gives $H_0 = 67.3$ [km/s Mpc], $w_1 = 0.4$ and $w_2 = -0.7$.

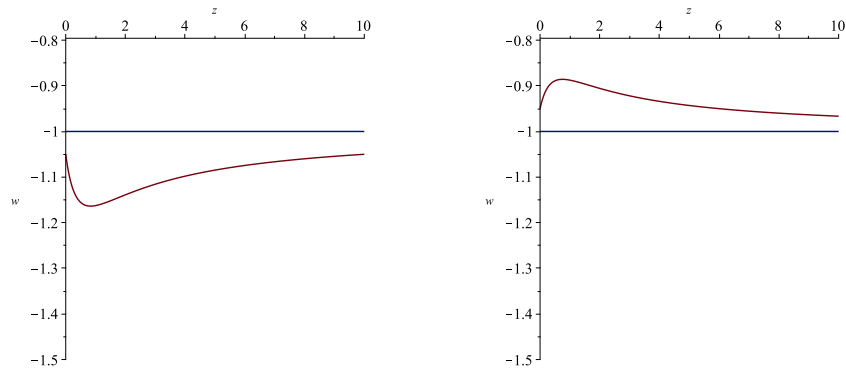


Figure 5: Redshift-dependences of w in the model of Taylor expansion. Left: the case of the standard distance ladder ($w_1 = -0.60$ and $w_2 = 1.1$). Right: the case of the inverse distance ladder ($w_1 = 0.4$ and $w_2 = -0.7$).

consistent with the results of rigorous fit results in [19] and [1], respectively. The corresponding redshift-dependences of w are shown in Fig.3. We see that the deviation from the Λ CDM model is larger for the case of the standard distance ladder than the case of inverse distance ladder. In other words we could say that the case of the inverse distance ladder essentially suggests the Λ CDM model and the case of the standard distance ladder suggests some new physics at low- z on the other hand.

Figs.4 and 5 show the same for the model of Taylor expansion of w . Though the shapes of $H(z)$ are almost the same of those in the CPL model, the redshift-dependence of w are different. In the model of Taylor expansion w quickly goes to -1 at larger values of redshift,

but it is not the case in the CPL model. Therefore, in view of modifying only low-redshift physics the model of Taylor expansion may be better. It is also noteworthy that $w < -1$ for the case of the standard distance ladder and $w \gtrsim -1$ for the case of the inverse distance ladder. Here, we note that these behaviors of w at larger redshift values are extrapolations depending on models which are constrained only by the data at low redshift values $z \lesssim 1$. Since the universe is dark energy dominant at $z \lesssim 1$, however, investigating the nature of dark energy with low-redshift data is reasonable at present status without precise information of the universe at larger redshift values.

In the next section we introduce the semi-analytic method to calculate angular power spectra C_ℓ^{EE} and C_ℓ^{BB} for $\ell \leq 11$ which has been developed in [25, 26, 27, 28, 29, 30, 31]. We utilize the approximation so called long wave length limit, or tight coupling limit [28, 32, 33, 34]. Though this approximation is rather drastic and rigorous quantitative precision is sacrificed, the resultant semi-analytic method clearly highlights the underlying physics. In section 3 we apply the method to the CPL models with the standard distance ladder and the inverse distance ladder, as well as for the models of Taylor expansion. We see that without model dependence (either the CPL model or the model of Taylor expansion) both $D_\ell^{EE} \equiv \ell(\ell + 1)C_\ell^{EE}/2\pi$ and $D_\ell^{BB} \equiv \ell(\ell + 1)C_\ell^{BB}/2\pi$ are somewhat enhanced with respect to the Λ CDM prediction at $8 < \ell < 11$ in case of the standard distance ladder, and slightly suppressed with respect to the Λ CDM prediction at $8 < \ell < 11$ in case of the inverse distance ladder. This indicate that future precise polarization measurements can give new information about the Hubble tension and physics beyond the Λ CDM model. In the last section we summarize our results and conclude. The readers who are not interested in the theoretical formalism can skip the next section and proceed to section 3.

2 The semi-analytic method

The reionization of the universe, which is expected to happen in the redshift period of $6 \lesssim z \lesssim 10$, gives free electrons by which CMB photons get Thomson scattering. In the presence of CMB perturbations such a Thomson scattering produces polarizations of CMB perturbations:

the scalar perturbation produces E-mode polarization and the tensor perturbation produces both E-mode and B-mode polarizations. Since the tensor perturbation, which has not yet been observed, is much smaller than the scalar perturbations, we concentrate on E-mode polarization by the scalar perturbation only neglecting the contribution of the tensor perturbation. In this work we set the tensor-to-scalar ratio as $r_{\text{TS}} = 0.03$.

We first introduce a semi-analytic method to calculate the angular power spectrum of E-mode polarization D_ℓ^{EE} due to scalar perturbations. We take the synchronous gauge:

$$ds^2 = a(\eta)^2 [d\eta^2 - (\delta_{ij} + h_{ij})dx^i dx^j], \quad (7)$$

where η is the conformal time and h_{ij} describes the perturbations around the background. The array of radiation strength is introduced as

$$\begin{pmatrix} I_\theta \\ I_\varphi \\ U \end{pmatrix} = \frac{h\nu^3}{c^2} \tilde{f}, \quad \tilde{f} = f_0(T_0, \nu) \left[\begin{pmatrix} 1 \\ 1 \\ 0 \end{pmatrix} + \tilde{f}_1 \right], \quad (8)$$

where I_θ and I_φ are intensities of the CMB radiation corresponding to two independent directions of polarizations and U is one of the Stokes parameters [35]. Other stokes parameters are described as $Q = I_\theta - I_\varphi$ and $V = 0$ (Thomson scattering does not produce circular polarizations). Since the CMB radiation is almost the blackbody radiation of temperature $T_0 \simeq 2.7[\text{K}]$ with small perturbations, we can write the array in this way using $f_0(T_0, \nu) = 1/(\exp(h\nu/k_B T_0) - 1)$ and an array of small perturbations \tilde{f}_1 . If we assume that the perturbation of intensity δI around the blackbody background I_0 is described as the temperature perturbation of the blackbody radiation intensity,

$$I_0 + \delta I = \frac{h\nu^3}{c^2} f_0(T_0 + \delta T, \nu) \simeq \frac{h\nu^3}{c^2} f_0(T_0, \nu) \left(1 - \gamma \frac{\delta T}{T_0} \right), \quad (9)$$

where

$$\gamma \equiv \frac{\nu}{f_0} \frac{\partial f_0}{\partial \nu}, \quad (10)$$

we may write the array of perturbations as $\tilde{f}_1 = \gamma \delta \tilde{f}$. Note that the perturbation $\delta \tilde{f}$ does not depend on the frequency of radiation, though γ is a function of frequency.

The Boltzmann equation (or the equation of radiation transfer divided by $h\nu^3/c^2$) is

$$\frac{\partial \tilde{f}}{\partial \eta} - \hat{n}_i \frac{\partial \tilde{f}}{\partial x^i} - \frac{1}{2} \frac{\partial h_{ij}}{\partial \eta} \hat{n}_i \hat{n}_j \nu \frac{\partial \tilde{f}}{\partial \nu} = -g(\eta) (\tilde{f} - \tilde{J}), \quad (11)$$

where $\hat{n} = (\sin \theta \cos \varphi, \sin \theta \sin \varphi, \cos \theta)$ is the unit vector pointing toward the sky in the direction of the photon to be observed, and

$$\tilde{J} = \frac{1}{4\pi} \int_{-1}^1 d\mu' \int_0^{2\pi} d\varphi' \tilde{P}(\mu, \varphi, \mu', \varphi') \tilde{f}(\mu, \mu') \quad (12)$$

which describes the effect of Thomson scattering, where $\mu \equiv \cos \theta$. The function $g(\eta) \equiv \sigma_T n_e(\eta) a(\eta)$, where σ_T is the Thomson scattering cross section and $n_e(\eta)$ is the density of free electrons, which are produced during reionization, describes the efficiency of the Thomson scattering. The third term of the left hand side of eq.(11) describes Sachs-Wolfe effect which is proportional to γ in the first order of perturbation (the first order in \tilde{f}_1 and h_{ij}).

Consider only the scalar perturbation of the background metric. The gauge-invariant primordial scalar perturbation is produced in the period of inflation as

$$\mathcal{R}^0(x) = \int \frac{d^3 k}{(2\pi)^3} \left(\hat{\alpha}_{\mathbf{k}} \mathcal{R}_k^0 e^{-i\mathbf{k} \cdot \mathbf{x}} + \hat{\alpha}_{\mathbf{k}}^\dagger (\mathcal{R}_k^0)^* e^{i\mathbf{k} \cdot \mathbf{x}} \right), \quad (13)$$

where $\hat{\alpha}_{\mathbf{k}}$ is the stochastic variable which satisfies $\langle \hat{\alpha}_{\mathbf{k}} \hat{\alpha}_{\mathbf{k}'}^\dagger \rangle = (2\pi)^3 \delta^3(\mathbf{k} - \mathbf{k}')$. The primordial power spectrum $P_{\mathcal{R}}(k)$ is defined as

$$\langle \mathcal{R}^0(x) \mathcal{R}^0(x) \rangle = \int_0^\infty \frac{dk}{k} \frac{k^3}{2\pi^2} |\mathcal{R}_k^0|^2 \equiv \int_0^\infty \frac{dk}{k} P_{\mathcal{R}}(k) \quad (14)$$

and its relevant parameterization is

$$P_{\mathcal{R}}(k) = A_S \left(\frac{k}{k_{\text{pivot}}} \right)^{n_s-1} \quad (15)$$

with $A_S \simeq 2.1 \times 10^{-9}$ and $n_s \simeq 0.965$ at $k_{\text{pivot}} = 0.05 \text{ [Mpc}^{-1}]$ which are determined by the PLANCK collaboration [1]. By solving evolution equations of scalar perturbations in synchronous gauge we obtain

$$\frac{\partial h_{ij}}{\partial \eta} = \frac{2}{15} \frac{\partial}{\partial x^i} \frac{\partial}{\partial x^j} \mathcal{R}^0(x) \quad (16)$$

which coincides with that given in [27] up to irrelevant overall sign.

The intensity perturbations are also expanded with the same stochastic variable as

$$\tilde{f}_1(x) = \int \frac{d^3 k}{(2\pi)^3} \left(\hat{\alpha}_{\mathbf{k}} \tilde{f}_{1k} e^{-i\mathbf{k} \cdot \mathbf{x}} + \hat{\alpha}_{\mathbf{k}}^\dagger (\tilde{f}_{1k})^* e^{i\mathbf{k} \cdot \mathbf{x}} \right), \quad (17)$$

and if we consider one component of scalar perturbations which propagates z direction: $\mathcal{R}_k^0 e^{-ikz}$, the Boltzmann equation becomes the equation for the corresponding component $\tilde{f}_{1k} e^{-ikz}$. Since there is a symmetry of rotation around z -axis in this case, $U = 0$, namely no B-mode polarizations. The matrix of the Thomson scattering in this case is [35]

$$P(\mu, \mu') = \frac{3}{4} \begin{pmatrix} 2(1 - \mu^2)(1 - \mu'^2) + \mu^2 \mu'^2 & \mu^2 \\ \mu'^2 & 1 \end{pmatrix}, \quad (18)$$

and the Boltzmann equation for the first order perturbations becomes

$$\left(\frac{\partial}{\partial \eta} + ik\mu + g(\eta) \right) \tilde{f}_{1k}(\eta, \mu, \nu) + \frac{\gamma}{15} \eta (k\mu)^2 \mathcal{R}_k^0 \begin{pmatrix} 1 \\ 1 \end{pmatrix} = g(\eta) \frac{1}{2} \int_{-1}^1 d\mu' P(\mu, \mu') \tilde{f}_{1k}(\eta, \mu', \nu). \quad (19)$$

Note that this equation depends on the observing frequency of the CMB, and the resultant amount of the polarizations depends on the frequency, because Sachs-Wolfe effect depends on the frequency. If we follow the assumption of eq.(9) and replace \tilde{f}_1 by $\gamma \delta \tilde{f}$, we have the Boltzmann equation which is independent from the frequency:

$$\left(\frac{\partial}{\partial \eta} + ik\mu + g(\eta) \right) \delta \tilde{f}_k(\eta, \mu) + \frac{1}{15} \eta (k\mu)^2 \mathcal{R}_k^0 \begin{pmatrix} 1 \\ 1 \end{pmatrix} = g(\eta) \frac{1}{2} \int_{-1}^1 d\mu' P(\mu, \mu') \delta \tilde{f}_k(\eta, \mu). \quad (20)$$

Now decompose the array of the perturbation as

$$\delta \tilde{f}_k = \alpha_k \begin{pmatrix} 1 \\ 1 \end{pmatrix} + \beta_k \begin{pmatrix} 1 \\ -1 \end{pmatrix}, \quad (21)$$

where α_k and β_k describe the perturbations of the total intensity and Stokes parameter Q , respectively. We obtain the equations

$$\left(\frac{\partial}{\partial \eta} + ik\mu + g(\eta) \right) \alpha_k(\eta, \mu) = -\frac{\mathcal{R}_k^0}{15} \eta (k\mu)^2 + g(\eta) \left\{ \alpha_{k,0} - \left(\mu^2 - \frac{1}{3} \right) G_k(\eta) \right\}, \quad (22)$$

$$\left(\frac{\partial}{\partial \eta} + ik\mu + g(\eta) \right) \beta_k(\eta, \mu) = g(\eta) (1 - \mu^2) G_k(\eta), \quad (23)$$

where

$$G_k(\eta) \equiv \frac{3}{4} (\beta_{k,0} - \alpha_{k,2} - \beta_{k,2}) \quad (24)$$

is the so called source function and

$$\alpha_k(\eta, \mu) = \sum_{\ell=0}^{\infty} (2\ell+1) \alpha_{k,\ell}(\eta) P_\ell(\mu), \quad \beta_k(\eta, \mu) = \sum_{\ell=0}^{\infty} (2\ell+1) \beta_{k,\ell}(\eta) P_\ell(\mu). \quad (25)$$

These eqs.(22) and (23) can be described in a different form as follows. The equations or $\alpha_{k,\ell}(\eta)$

$$\dot{\alpha}_{k,0} = -ik\alpha_{k,1} - \frac{\mathcal{R}_k^0}{45} \eta k^2, \quad (26)$$

$$\dot{\alpha}_{k,1} = -ik \left(\frac{1}{3} \alpha_{k,0} + \frac{2}{3} \alpha_{k,2} \right) - g\alpha_{k,1}, \quad (27)$$

$$\dot{\alpha}_{k,2} = -ik \left(\frac{2}{5} \alpha_{k,1} + \frac{3}{5} \alpha_{k,3} \right) - \frac{2}{5} \frac{\mathcal{R}_k^0}{45} \eta k^2 - g \frac{1}{10} (9\alpha_{k,2} + \beta_{k,0} - \beta_{k,2}), \quad (28)$$

$$\dot{\alpha}_{k,\ell} = -ik \left(\frac{\ell}{2\ell+1} \alpha_{k,\ell-1} + \frac{\ell+1}{2\ell+1} \alpha_{k,\ell+1} \right) - g\alpha_{k,\ell}, \quad \ell \geq 3, \quad (29)$$

where dots indicate derivatives by η , and the equations for $\beta_{k,\ell}(\eta)$

$$\dot{\beta}_{k,0} = -ik\beta_{k,1} - g \frac{1}{2} (\beta_{k,0} + \alpha_{k,2} + \beta_{k,2}), \quad (30)$$

$$\dot{\beta}_{k,1} = -ik \left(\frac{1}{3} \beta_{k,0} + \frac{2}{3} \beta_{k,2} \right) - g\beta_{k,1}, \quad (31)$$

$$\dot{\beta}_{k,2} = -ik \left(\frac{2}{5}\beta_{k,1} + \frac{3}{5}\beta_{k,3} \right) - g \frac{1}{10} (9\beta_{k,2} + \beta_{k,0} - \alpha_{k,2}), \quad (32)$$

$$\dot{\beta}_{k,\ell} = -ik \left(\frac{\ell}{2\ell+1}\beta_{k,\ell-1} + \frac{\ell+1}{2\ell+1}\beta_{k,\ell+1} \right) - g\beta_{k,\ell}, \quad \ell \geq 3. \quad (33)$$

The solution of eq.(23) can be formally written as

$$\beta_k = \int_0^\eta d\eta' e^{-\kappa(\eta,\eta')} e^{-ik\mu(\eta-\eta')} g(\eta') (1-\mu^2) G_k(\eta'), \quad (34)$$

where

$$\frac{\partial}{\partial \eta} \kappa(\eta, \eta') = g(\eta), \quad \text{and} \quad \kappa(\eta, \eta) = 0. \quad (35)$$

By using the formula

$$e^{ikr\mu} = \sum_{m=0}^{\infty} (2m+1) i^m j_m(kr) P_m(\mu), \quad (36)$$

where $j_\ell(x)$ is the spherical Bessel function, the solution becomes

$$\begin{aligned} \beta_{k,\ell} = & \int_0^\eta d\eta' e^{-\kappa(\eta,\eta')} g(\eta') G_k(\eta') i^\ell \left\{ \frac{\ell(\ell-1)}{(2\ell+1)(2\ell-1)} j_{\ell-2}(k(\eta'-\eta)) \right. \\ & \left. + \frac{2(\ell^2+\ell-1)}{(2\ell+3)(2\ell-1)} j_\ell(k(\eta'-\eta)) + \frac{(\ell+2)(\ell+1)}{(2\ell+3)(2\ell+1)} j_{\ell+2}(k(\eta'-\eta)) \right\}. \end{aligned} \quad (37)$$

This form indicates that $\beta_{k,\ell}$ can be obtained, once the source function has been given.

In general two kinds of polarizations, E-mode and B-mode, are originated from the fact that the polarization tensor (here, all its components are small perturbations of the CMB) is decomposed in corresponding two scalar components as

$$P_{ab}(\hat{n}) = \frac{1}{2} \begin{pmatrix} Q & -U \sin \theta \\ -U \sin \theta & -Q \sin^2 \theta \end{pmatrix} = \sum_{\ell=2}^{\infty} \sum_{m=-\ell}^{\ell} [a_{\ell m}^E Y_{(\ell m)ab}^E(\hat{n}) + a_{\ell m}^B Y_{(\ell m)ab}^B(\hat{n})], \quad (38)$$

where $Y_{(\ell m)ab}^E(\hat{n})$ and $Y_{(\ell m)ab}^B(\hat{n})$ are two independent spherical harmonic functions on the sphere (see [36] for a review). The coefficients $a_{\ell m}^E$ and $a_{\ell m}^B$ are given as

$$a_{\ell m}^E = \sqrt{\frac{2(\ell-2)!}{(\ell+2)!}} \int d\hat{n} \nabla_a \nabla_b P^{ab}(\hat{n}) (Y_\ell^m(\hat{n}))^*,$$

$$a_{\ell m}^B = \sqrt{\frac{2(\ell-2)!}{(\ell+2)!}} \int d\hat{n} \nabla_a \nabla_c P^{ab}(\hat{n}) \epsilon^c_b (Y_\ell^m(\hat{n}))^*, \quad (39)$$

where $d\hat{n} = d\theta \sin\theta d\varphi$, ∇_a is the covariant derivative on the sphere, $Y_\ell^m(\hat{n})$ is the spherical harmonic function. If we consider the component Q as a perturbation that follows eq.(9) with an additional factor 2, we have $Q_k = T_0 \beta_k$ in the unit of temperature from $Q = I_\theta - I_\varphi$, where

$$Q(x) = \int \frac{d^3k}{(2\pi)^3} \left(\hat{\alpha}_{\mathbf{k}} Q_k e^{-i\mathbf{k}\cdot\mathbf{x}} + \hat{\alpha}_{\mathbf{k}}^\dagger (Q_k)^* e^{i\mathbf{k}\cdot\mathbf{x}} \right). \quad (40)$$

In the present background of scalar perturbation, $\mathcal{R}_k^0 e^{-ikz}$, we can describe the component $a_{k,\ell m}^E$ by $\beta_{k,\ell}$ as

$$\begin{aligned} a_{k,\ell m}^E = & - \delta_{m0} T_0 \sqrt{\pi(2\ell+1)} \sqrt{\frac{2\ell(\ell-1)}{(\ell+1)(\ell+2)}} \beta_{k,\ell} \\ & + \delta_{m0} T_0 \sqrt{\pi(2\ell+1)} \sqrt{\frac{2\ell(\ell-1)}{(\ell+1)(\ell+2)}} \sum_{n=1}^{[\ell/2]} \frac{2(\ell-2n)+1}{\ell(\ell-1)/2} \beta_{k,\ell-2n}, \end{aligned} \quad (41)$$

where we have made a resummation by which the infinite summation becomes that of the finite range [31]. The angular power spectrum for the E-mode polarization is given by

$$C_\ell^{EE} = \int \frac{d^3k}{(2\pi)^3} \frac{1}{2\ell+1} \sum_{m=-\ell}^{\ell} |a_{k,\ell m}^E|^2, \quad (42)$$

where we assume the isotropy of the universe.

Here, we consider long wavelength limit in which we neglect the terms with $-ik$ in equations for $\alpha_{k,\ell}$ and $\beta_{k,\ell}$.

$$\dot{\alpha}_{k,0} \simeq -\frac{\mathcal{R}_k^0}{45} \eta k^2, \quad (43)$$

$$\dot{\alpha}_{k,1} \simeq -g\alpha_{k,1}, \quad (44)$$

$$\dot{\alpha}_{k,2} \simeq -\frac{2}{5} \frac{\mathcal{R}_k^0}{45} \eta k^2 - g \frac{1}{10} (9\alpha_{k,2} + \beta_{k,0} - \beta_{k,2}), \quad (45)$$

$$\dot{\alpha}_{k,\ell} \simeq -g\alpha_{k,\ell}, \quad \ell \geq 3, \quad (46)$$

$$\dot{\beta}_{k,0} \simeq -g \frac{1}{2} (\beta_{k,0} + \alpha_{k,2} + \beta_{k,2}), \quad (47)$$

$$\dot{\beta}_{k,1} \simeq -g\beta_{k,1}, \quad (48)$$

$$\dot{\beta}_{k,2} \simeq -g\frac{1}{10}(9\beta_{k,2} + \beta_{k,0} - \alpha_{k,2}) \quad (49)$$

$$\dot{\beta}_{k,\ell} \simeq -g\beta_{k,\ell}, \quad \ell \geq 3. \quad (50)$$

Moreover, neglect $\alpha_{k,\ell}$ and $\beta_{k,\ell}$ of $\ell = 1$ and $\ell \geq 3$ considering that they are all exponentially smaller than the others (so called tight coupling limit), then we can obtain a differential equation of the source function

$$\dot{G}_k = -\frac{3}{10}gG_k + \frac{\mathcal{R}_k^0}{150}k^2\eta. \quad (51)$$

The solution of this equation can be formally written as

$$G_k \simeq \frac{1}{10} \int_0^\eta d\eta' e^{-\frac{3}{10}\kappa(\eta,\eta')} \frac{\mathcal{R}_k^0}{15} k^2 \eta'. \quad (52)$$

Since we set that the source function vanishes at the time when the reionization starts, η_{ion} , and the exponential factor in the integrant is almost always unity in good approximation [34], we obtain an approximate source function

$$G_k \simeq \frac{\mathcal{R}_k^0}{300} k^2 (\eta^2 - \eta_{\text{ion}}^2). \quad (53)$$

Then, from eq.(37) in the same approximation we obtain

$$\begin{aligned} \beta_{k,\ell} \simeq & \int_{\eta_{\text{ion}}}^\eta d\eta' g(\eta') \frac{\mathcal{R}_k^0}{300} k^2 (\eta'^2 - \eta_{\text{ion}}^2) i^\ell \left\{ \frac{\ell(\ell-1)}{(2\ell+1)(2\ell-1)} j_{\ell-2}(k(\eta' - \eta)) \right. \\ & \left. + \frac{2(\ell^2 + \ell - 1)}{(2\ell+3)(2\ell-1)} j_\ell(k(\eta' - \eta)) + \frac{(\ell+2)(\ell+1)}{(2\ell+3)(2\ell+1)} j_{\ell+2}(k(\eta' - \eta)) \right\}. \end{aligned} \quad (54)$$

In this way we obtain an approximate formula for E-mode angular power spectrum from this result and eqs.(41) and (42). We have used the approximation to obtain $\beta_{k,\ell}$ through the approximate source function without fully solving the equations for all $\beta_{k,\ell}$.

Exactly the same story applies to the B-mode angular power spectrum by tensor perturbations (see [34] for details). Here, we simply give results. The B-mode angular power spectrum

due to tensor perturbations is given as

$$C_\ell^{\text{BB}} = 2 \int \frac{d^3k}{(2\pi)^3} \frac{1}{2\ell+1} \sum_m |a_{\ell m}^{\text{B}}(k)|^2 = T_0^2 \frac{4}{\pi} \int dk k^2 \left| \frac{\ell+2}{2\ell+1} \beta_{k,\ell-1} + \frac{\ell-1}{2\ell+1} \beta_{k,\ell+1} \right|^2, \quad (55)$$

where $\beta_{k,\ell}$ is now approximately given as

$$\beta_{k,\ell}(\eta_0) \simeq \int_{\eta_{\text{ion}}}^{\eta_0} d\eta' i^\ell j_\ell(k(\eta' - \eta_0)) g(\eta') G_k(\eta'), \quad (56)$$

$$G_k(\eta) \simeq -\frac{1}{10} (D_k(\eta) - D_k(\eta_{\text{ion}})). \quad (57)$$

Here, the source function is described by the amplitude of tensor perturbations in the metric of eq.(7) as

$$h_{ij}(x) = \int \frac{d^3k}{(2\pi)^3} \sum_{a=+,\times} \left(\hat{\beta}_{\mathbf{k}} e_{ij}^a D_k(\eta) e^{-i\mathbf{k}\cdot\mathbf{x}} + \hat{\beta}_{\mathbf{k}}^\dagger (e_{ij}^a)^\dagger (D_k)^* e^{i\mathbf{k}\cdot\mathbf{x}} \right), \quad (58)$$

where $\hat{\beta}_{\mathbf{k}}$ is another stochastic variable which satisfies $\langle \hat{\beta}_{\mathbf{k}} \hat{\beta}_{\mathbf{k}'}^\dagger \rangle = (2\pi)^3 \delta^3(\mathbf{k} - \mathbf{k}')$ and

$$D_k(\eta) = \sqrt{\frac{2\pi^2 A_T}{k^3}} \cdot 3 \sqrt{\frac{\pi}{2}} (k\eta)^{-3/2} J_{3/2}(k\eta) \quad (59)$$

which is the solution of the evolution equation of tensor perturbations ($J_n(x)$ is the Bessel function) corresponding to the initial condition, namely, the power spectrum of the primordial tensor perturbation

$$P_{\mathcal{T}} = A_T \left(\frac{k}{k_{\text{pivot}}} \right)^{n_T} \quad (60)$$

with $A_T = r_{TS} A_S$, $r_{TS} = 0.03$ and $n_T = 0$. There is no deep reason to choose these values, and it is simply a set of test values, because primordial tensor perturbation has not yet been observed.

3 The results and implications

In this section we discuss the angular power spectra of the E-mode and B-mode CMB polarizations which are produced by Thomson scattering of CMB photons in the period of reionization. Our main concern is how the power spectra are affected by the difference of the expansion of the universe that we have discussed in the first section. The angular power spectra corresponding to two models which are suggested by the standard distance ladder and the inverse distance ladder are calculated, respectively, and they are compared with those of the concordance Λ CDM model. The essential difference of these two models is the way of expanding the universe in the period of reionization.

In the semi-analytic method, which has been introduced in the previous section, the difference of the behavior of the function $g(\eta) = \sigma_T n_e(\eta) a(\eta)$ is essential, where σ_T is the Thomson scattering cross section, $n_e(\eta)$ is the time-dependent number density of free electrons, and $a(\eta)$ is the scale factor. It can be understood that this function $g(\eta)$ represents the efficiency of producing polarizations at each time. Note that $n_e(\eta) \propto a(\eta)^{-3}$ and the optical depth

$$\tau \simeq \int_{\eta_{\text{ion}}}^{\eta_0} d\eta' g(\eta') \quad (61)$$

has been measured as $\tau = 0.054 \pm 0.007$ by the PLANCK collaboration [1]. The behavior of $n_e(\eta)a(\eta)^3$ shows the genuine evolution of free electron density without the effect of dilution by the expansion of the universe. Though the knowledge of the evolution has not yet been established, we know that the reionization is finished until $z = 6$ by the observation of Lyman- α forest and Gunn-Peterson trough [37], and its main process starts around $z \simeq 8$. We set η_{ion} to the time corresponding to the redshift $z_{\text{ion}} = 8$, namely $a(\eta_{\text{ion}}) = 1/9$, applying the relation $1 + z = 1/a$ with the normalization $a(\eta_0) = 1$, which is also the condition to set the value of η_0 , the age of the universe. In this work we simply assume

$$n_e(\eta)a(\eta)^3 = n_e^{\text{ion}} \tanh\left(20 \frac{\eta - \eta_{\text{ion}}}{\eta_{\text{ion}}}\right), \quad (62)$$

where $\eta \geq \eta_{\text{ion}}$ and n_e^{ion} is a constant which should be determined by eq.(61) with $\tau = 0.054$.

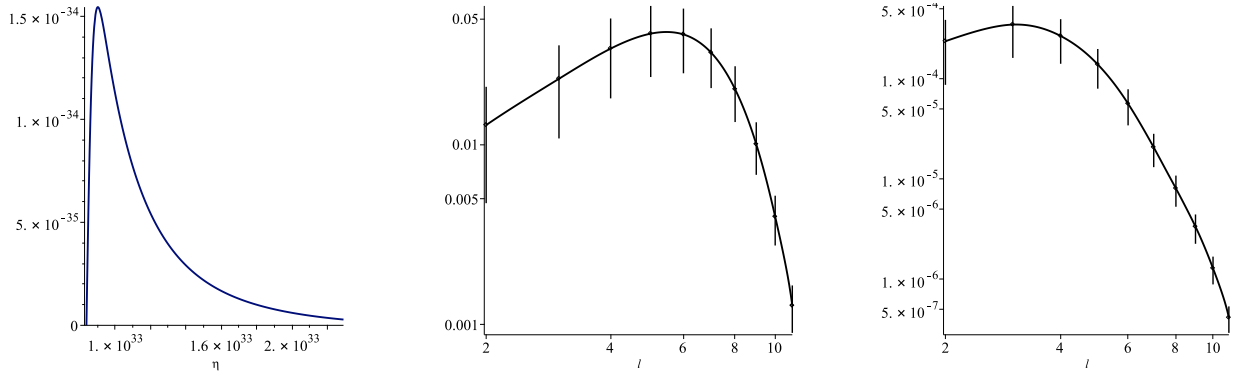


Figure 6: The function g and angular power spectra for the Λ CDM model. Left: g [eV] as a function of conformal time η [eV^{-1}] in the region $\eta_{\text{ion}} < \eta < \eta_0$. Middle: the angular power spectrum of E-mode polarization D_ℓ^{EE} [μK^2] with errors by cosmic variance. Right: the angular power spectrum of B-mode polarization D_ℓ^{BB} [μK^2] with errors by cosmic variance.

A numerical number 20 has been chosen so that about 90% of reionization has been finished at $z = 6$ in our models.

First, we fix the function in case of the Λ CDM model and calculate the E-mode and B-mode power spectra. Our concordance Λ CDM model is defined by eq.(4) with $w_0 = -1$, $w_a = 0$, $H_0 = 67.4$ [km/s Mpc], $\Omega_m = 0.3$ and $\Omega_{\text{DE}} = 1 - \Omega_m = 0.7$. This is the first order differential equation for the scale factor, and we solve it with the initial condition $a(\eta = 0) = 0$. In fig.6 we present the function g and angular power spectra in the Λ CDM model. The plot of the function g indicates that the efficiency to produce polarizations quickly increases as the increase of the free electron density just after reionization starts, and then the efficiency rather quickly decreases as the decrease of the free electron density by the expansion of the universe. Both E-mode and B-mode angular power spectra roughly reflect this behavior: larger ℓ powers, which have produced at early time, are small, and then they become larger for smaller ℓ , but lower ℓ powers, which have produced at late time, become small again. Although our approximation is rather drastic, the resultant power spectra are in rather good agreement with more rigorous calculations in not only their shapes but also even quantitatively. We assume the cosmic variance limited measurement and the corresponding errors are included in the plots in fig.6.

In fig.7 we present the results in the CPL model with the standard distance ladder. There is a clear difference in the function g between this model and the Λ CDM model. The peak

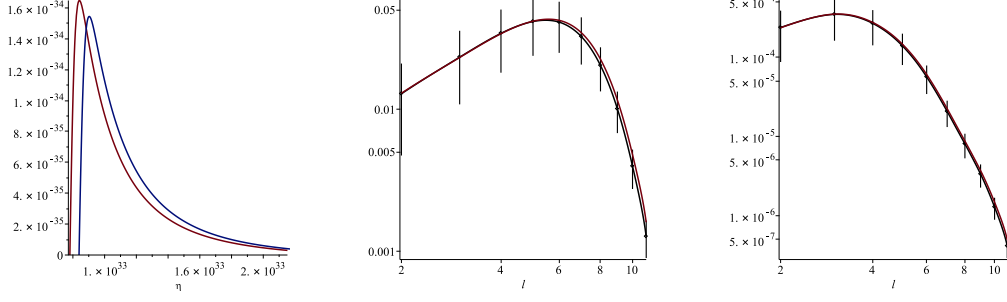


Figure 7: The function g and angular power spectra for the CPL model with the standard distance ladder. Left: g [eV] as a function of conformal time η [eV $^{-1}$] in the region $\eta_{\text{ion}} < \eta < \eta_0$. The line with higher peak is that of this model being compared with that of the Λ CDM model. Middle: the angular power spectra of E-mode polarization D_ℓ^{EE} [μK^2] with errors by cosmic variance. The spectrum of this model almost overlaps with that of the Λ CDM model with some excess at high ℓ . Right: the angular power spectra of B-mode polarization D_ℓ^{BB} [μK^2] with errors by cosmic variance. The spectrum of this model almost overlaps with that of the Λ CDM model with some excess at high ℓ .

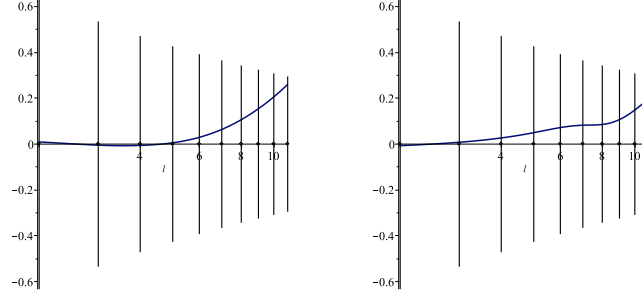


Figure 8: The difference of the angular power spectra in the CPL model with the standard distance ladder and that in the Λ CDM model. Left: plot of $(D_\ell^{EE} - D_\ell^{EE,\Lambda\text{CDM}})/D_\ell^{EE,\Lambda\text{CDM}}$ with errors by cosmic variance in vertical lines. Right: plot of $(D_\ell^{BB} - D_\ell^{BB,\Lambda\text{CDM}})/D_\ell^{BB,\Lambda\text{CDM}}$ with errors by cosmic variance in vertical lines.

becomes higher and every behaviors become quicker, because the time to start reionization is earlier, the age of the universe becomes shorter, and the period of reionization $\eta_0 - \eta_{\text{ion}}$ becomes shorter. Note that the function g is constrained by eq.(61). As the result at larger ℓ the values of both D_ℓ^{EE} and D_ℓ^{BB} are enhanced, though the values at smaller ℓ are not changed. This change of the shape of the angular power spectra are clearly seen in fig.8. Note that this magnitude of distortion of the angular power spectra about 20% does not happen by simply changing the value of H_0 keeping $w = -1$. For example, if we simply change the value of H_0 from 67.4 to 74.0 [km/s Mpc] with fixed $w = -1$, the change of both E-mode and B-mode power spectra is less than 1%.

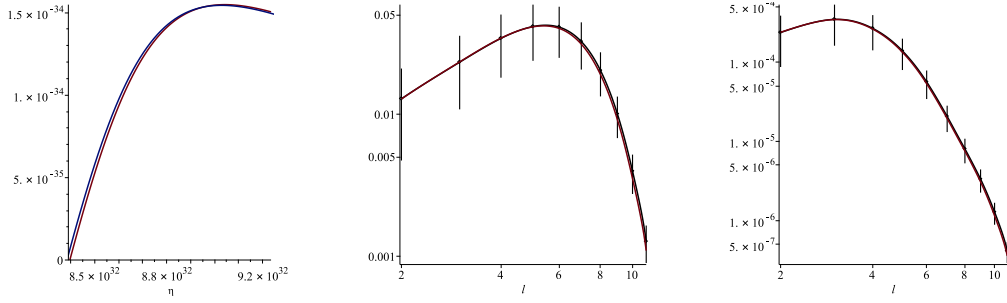


Figure 9: The function g and angular power spectra for the CPL model with the inverse distance ladder. Left: g [eV] as a function of conformal time η [eV $^{-1}$] in the region of η close to η_{ion} . The lines corresponding to the model with the inverse distance ladder and the Λ CDM model almost overlap with very little shift of the former to the right in η . Middle: the angular power spectra of E-mode polarization D_ℓ^{EE} [μK^2] with errors by cosmic variance. The spectrum of this model almost overlaps with that of the Λ CDM model with some suppression at high ℓ (difficult to see with eyes). Right: the angular power spectra of B-mode polarization D_ℓ^{BB} [μK^2] with errors by cosmic variance. The spectrum of this model almost overlaps with that of the Λ CDM model with some suppression at high ℓ (difficult to see with eyes).

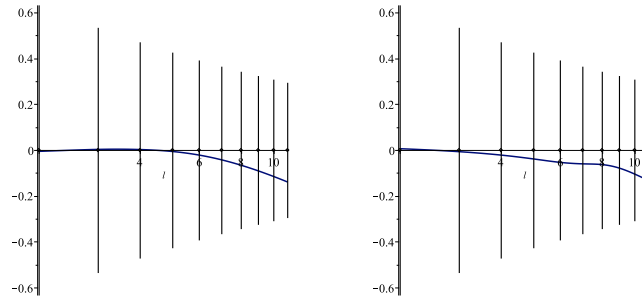


Figure 10: The difference of the angular power spectra in the CPL model with the inverse distance ladder and that in the Λ CDM model. Left: plot of $(D_\ell^{EE} - D_\ell^{EE,\Lambda\text{CDM}})/D_\ell^{EE,\Lambda\text{CDM}}$ with errors by cosmic variance in vertical lines. Right: plot of $(D_\ell^{BB} - D_\ell^{BB,\Lambda\text{CDM}})/D_\ell^{BB,\Lambda\text{CDM}}$ with errors by cosmic variance in vertical lines.

In fig.9 we present the results in the CPL model with the inverse distance ladder. The difference in the function g is small as expected, which comes from that reionization starts slightly later and the age of the universe becomes slightly shorter. Since the difference is little, the change of angular power spectra is very small. The change can be only seen in the plots of fig.10, which shows that the powers at larger ℓ become smaller. Note that this behavior is opposite to that in the model with the standard distance ladder. This little dump comes from slightly later start of reionization. Since the difference from the Λ CDM model is small, we may interpret this result as that the data set of the inverse distance ladder favors the Λ CDM model, or dark energy as a cosmological constant.

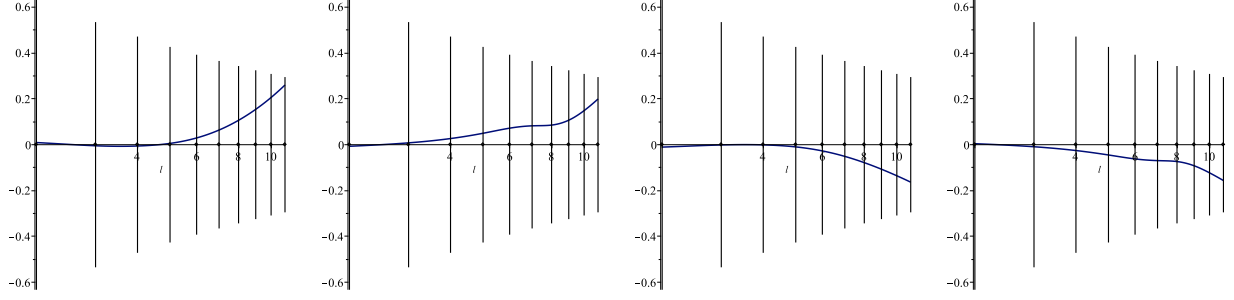


Figure 11: The difference of the angular power spectra in the model of Taylor expansion with the standard distance ladder and the inverse distance ladder and that in the Λ CDM model. Left: plot of $(D_\ell^{EE} - D_\ell^{EE,\Lambda\text{CDM}})/D_\ell^{EE,\Lambda\text{CDM}}$ in the model with the standard distance ladder. Middle-Left: plot of $(D_\ell^{BB} - D_\ell^{BB,\Lambda\text{CDM}})/D_\ell^{BB,\Lambda\text{CDM}}$ in the model with the standard distance ladder. Middle-Right: plot of $(D_\ell^{EE} - D_\ell^{EE,\Lambda\text{CDM}})/D_\ell^{EE,\Lambda\text{CDM}}$ in the model with the inverse distance ladder. Right: plot of $(D_\ell^{BB} - D_\ell^{BB,\Lambda\text{CDM}})/D_\ell^{BB,\Lambda\text{CDM}}$ in the model with the inverse distance ladder. In all plots vertical lines indicate errors by cosmic variance.

Fig.11 shows that we have completely the same result in the models of Taylor expansion, which leads a model independent observation: in the production of the polarizations of the CMB in the period of reionization with non-trivially time-dependent equation of state of dark energy, the evolution of the universe suggested by the standard distance ladder indicates higher polarization powers at larger ℓ , and the evolution of the universe suggested by the inverse distance ladder indicates lower polarization powers at larger ℓ . This means that the future precise measurements of E-mode and possibly B-mode angular power spectra at low- ℓ by LiteBIRD, for example, can give a useful information to the Hubble tension. Suppose that we find higher polarization powers in future experiments. It can be understood that the non-trivially time-dependent equation of state of dark energy with the standard distance ladder, namely larger value of the Hubble constant with new physics at low- z , is favored.

Before closing this section we discuss the effect of ambiguity of our knowledge of reionization. Fig.12 shows how angular power spectra change depending on the value of the optical depth τ and the value of the redshift z_{ion} when reionization starts. The ambiguity of the optical depth by the PLANCK collaboration causes the change of power spectra within cosmic variance. The lack of the knowledge about reionization process gives larger distortions beyond cosmic variance, and it is important to obtain the knowledge by exploring deeper universe through future observations of quasars, 21-cm hyperfine line of hydrogen, and so on. Since we have to

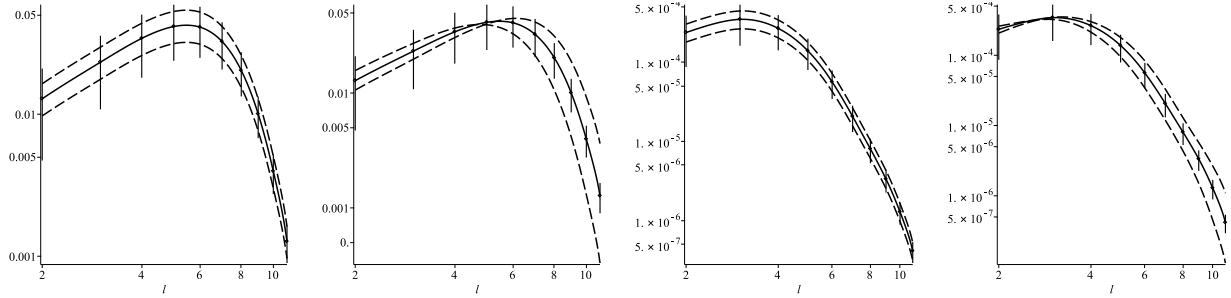


Figure 12: The ambiguities of angular power spectra under changing the value of optical depth τ and the value of redshift z_{ion} when reionization starts. Left: D_{ℓ}^{EE} with different values of $\tau = 0.054 \pm 0.007$. Three lines are corresponding to those of the upper bound value, center value and lower bound value, from up to down, respectively. Middle-Left: D_{ℓ}^{EE} with different value of z_{ion} . Three lines are corresponding to the values of $z_{\text{ion}} = 7, 8$, and 9 , from down to up at $\ell = 10$, respectively. Middle-Right: D_{ℓ}^{BB} with different values of $\tau = 0.054 \pm 0.007$. Three lines are corresponding to those of the upper bound value, center value and lower bound value, from up to down, respectively. Right: D_{ℓ}^{BB} with different value of z_{ion} . Three lines are corresponding to the values of $z_{\text{ion}} = 7, 8$, and 9 , from down to up at $\ell = 10$, respectively.

confront cosmic variance at low- ℓ , the precise knowledge of reionization is necessary as well as more precise theoretical calculations of polarization power spectra.

4 Conclusions

There are many ways to measure the Hubble constant, the present expansion rate of the universe, and at present these results do not converge to a single preferable value within errors. This problem so called Hubble tension may indicate something about dark energy of the universe which can change the way of expanding the universe. We have concentrated on the possibility that some physics at lower redshift, around the period of reionization, may give a solution of the Hubble tension. Many measurements of the Hubble parameter at various values of redshift suggest the history of expansion of the universe at lower redshift. An important observation is that the measurements of the Hubble parameter at various redshifts can be categorized into two groups depending on how the distance is determined: by the standard distance ladder or the inverse distance ladder [4]. We have made a simple fit of the Hubble parameter as a function of redshift, by using only the data with the standard distance ladder or only the data with the inverse distance ladder. In these fits we have introduced two phenomenological models of

the equation of state of dark energy as a function of redshift: one is the CPL model and the other is the model of Taylor expansion. Therefore, we have obtained four different data-driven phenomenological models of dark energy.

The polarizations of the CMB at low $\ell \lesssim 10$ are mainly produced through the Thomson scattering of the CMB photons off the free electrons which are produced during reionization. The time evolution of the free electron density is determined by the reionization process as well as the way of expanding the universe in the period of the redshift $z \lesssim 10$. Although our data-driven phenomenological models have been obtained by the data in the range of redshift $0 \lesssim z \lesssim 1$, we have assumed that they can be applied to the period of reionization by extrapolations. We have developed the semi-analytic method to calculate the angular power spectrum of the E-mode polarization of the CMB due to scalar perturbations with long wavelength limit, which is almost the same method in an author's previous work for the B-mode polarization due to tensor perturbations [34]. The angular power spectra of E-mode and B-mode polarizations due to scalar and tensor perturbations, respectively, have been calculated in our four phenomenological models using this semi-analytic method. We have compared the results with the prediction of the concordance Λ CDM model.

The two models with the standard distance ladder give the angular power spectra which are somewhat enhanced at larger ℓ . On the other hand, the two models with the inverse distance ladder give the angular power spectra which are slightly suppressed at larger ℓ . There is no model dependence, whether the CPL model or the model of Taylor expansion, in this results, though their redshift dependences of the equation of state of dark energy are not exactly the same in the period of reionization. This is because in that period the universe is in the era of matter dominant and the contribution of the difference is little. The important difference for the result is whether w is smaller or larger than -1 at smaller redshift, corresponding to the models with the standard distance ladder and the inverse distance ladder, respectively. These arguments lead us to a model independent observation that in the production of the polarizations of the CMB in the period of reionization with non-trivially time-dependent equation of state of dark energy, the evolution of the universe suggested by the standard distance ladder

indicates higher polarization powers at larger ℓ , and the evolution of the universe suggested by the inverse distance ladder indicates lower polarization powers at larger ℓ , than the prediction of the concordance Λ CDM model. Therefore, future precise measurements of low- ℓ polarizations of the CMB by LiteBIRD, for example, may provide some indication to the Hubble tension. In addition to the cosmic variance limited measurements it is also necessary to provide precise knowledge of the reionization process, the value of optical depth, the time to start reionization, and so on. Even as of today more precise fits of Hubble parameter with more possible data in both with the standard and inverse distance ladders, and more precise numerical calculations of angular power spectra of CMB polarizations are worth to pursue this observation further. Furthermore, discussion about practical measurements in future experiments (signal-to-noise ratio, for example) requires to include by numerical calculations other contributions to polarizations: E-mode polarizations which are produced at the period of recombination and B-mode polarizations which are produced by the lensing effect from E-mode polarizations. We leave this analysis for future work.

Acknowledgments

The author would like to thank A. Gruppuso for helpful comments. This work was supported in part by JSPS KAKENHI Grant Number 19K03851.

References

- [1] N. Aghanim *et al.* [Planck], “Planck 2018 results. VI. Cosmological parameters,” [arXiv:1807.06209 [astro-ph.CO]].
- [2] A. G. Riess, S. Casertano, W. Yuan, L. M. Macri and D. Scolnic, “Large Magellanic Cloud Cepheid Standards Provide a 1% Foundation for the Determination of the Hubble Constant and Stronger Evidence for Physics beyond Λ CDM,” *Astrophys. J.* **876** (2019) no.1, 85 [arXiv:1903.07603 [astro-ph.CO]].

- [3] W. L. Freedman, B. F. Madore, T. Hoyt, I. S. Jang, R. Beaton, M. G. Lee, A. Monson, J. Neeley and J. Rich, “Calibration of the Tip of the Red Giant Branch (TRGB),” [arXiv:2002.01550 [astro-ph.GA]].
- [4] A. J. Cuesta, L. Verde, A. Riess and R. Jimenez, “Calibrating the cosmic distance scale ladder: the role of the sound horizon scale and the local expansion rate as distance anchors,” *Mon. Not. Roy. Astron. Soc.* **448** (2015) no.4, 3463 [arXiv:1411.1094 [astro-ph.CO]].
- [5] O. H. Philcox, M. M. Ivanov, M. Simonović and M. Zaldarriaga, “Combining Full-Shape and BAO Analyses of Galaxy Power Spectra: A 1.6% CMB-independent constraint on H_0 ,” *JCAP* **05** (2020), 032 [arXiv:2002.04035 [astro-ph.CO]].
- [6] F. Bianchini *et al.* [SPT], “Constraints on Cosmological Parameters from the 500 deg² SPTpol Lensing Power Spectrum,” *Astrophys. J.* **888** (2020), 119 [arXiv:1910.07157 [astro-ph.CO]].
- [7] D. Pesce, J. Braatz, M. Reid, A. Riess, D. Scolnic, J. Condon, F. Gao, C. Henkel, C. Impellizzeri, C. Kuo and K. Lo, “The Megamaser Cosmology Project. XIII. Combined Hubble constant constraints,” *Astrophys. J. Lett.* **891** (2020) no.1, L1 [arXiv:2001.09213 [astro-ph.CO]].
- [8] K. C. Wong, S. H. Suyu, G. C. F. Chen, C. E. Rusu, M. Millon, D. Sluse, V. Bonvin, C. D. Fassnacht, S. Taubenberger, M. W. Auger, S. Birrer, J. H. Chan, F. Courbin, S. Hilbert, O. Tihhonova, T. Treu, A. Agnello, X. Ding, I. Jee, E. Komatsu, A. J. Shajib, A. Sonnenfeld, R. D. Blandford, L. V. Koopmans, P. J. Marshall and G. Meylan, “H0LiCOW XIII. A 2.4% measurement of H_0 from lensed quasars: 5.3 σ tension between early and late-Universe probes,” [arXiv:1907.04869 [astro-ph.CO]].
- [9] M. Raveri, “Reconstructing Gravity on Cosmological Scales,” *Phys. Rev. D* **101** (2020) no.8, 083524 [arXiv:1902.01366 [astro-ph.CO]].

- [10] E. Di Valentino, A. Melchiorri and J. Silk, “Planck evidence for a closed Universe and a possible crisis for cosmology,” *Nature Astron.* **4** (2019) no.2, 196-203 [arXiv:1911.02087 [astro-ph.CO]].
- [11] W. Handley, “Curvature tension: evidence for a closed universe,” [arXiv:1908.09139 [astro-ph.CO]].
- [12] G. Efstathiou and S. Gratton, “The evidence for a spatially flat Universe,” [arXiv:2002.06892 [astro-ph.CO]].
- [13] E. Di Valentino, A. Melchiorri and J. Silk, “Cosmic Discordance: Planck and luminosity distance data exclude Λ CDM,” [arXiv:2003.04935 [astro-ph.CO]].
- [14] S. Vagnozzi, E. Di Valentino, S. Gariazzo, A. Melchiorri, O. Mena and J. Silk, “Listening to the BOSS: the galaxy power spectrum take on spatial curvature and cosmic concordance,” [arXiv:2010.02230 [astro-ph.CO]].
- [15] S. Vagnozzi, A. Loeb and M. Moresco, “Eppur è piatto? The cosmic chronometer take on spatial curvature and cosmic concordance,” [arXiv:2011.11645 [astro-ph.CO]].
- [16] L. Knox and M. Millea, *Phys. Rev. D* **101** (2020) no.4, 043533 [arXiv:1908.03663 [astro-ph.CO]].
- [17] M. Chevallier and D. Polarski, “Accelerating universes with scaling dark matter,” *Int. J. Mod. Phys. D* **10** (2001), 213-224 [arXiv:gr-qc/0009008 [gr-qc]].
- [18] E. V. Linder, “Exploring the expansion history of the universe,” *Phys. Rev. Lett.* **90** (2003), 091301 [arXiv:astro-ph/0208512 [astro-ph]].
- [19] A. G. Riess, S. A. Rodney, D. M. Scolnic, D. L. Shafer, L. G. Strolger, H. C. Ferguson, M. Postman, O. Graur, D. Maoz, S. W. Jha, B. Mobasher, S. Casertano, B. Hayden, A. Molino, J. Hjorth, P. M. Garnavich, D. O. Jones, R. P. Kirshner, A. M. Koekemoer, N. A. Grogin, G. Brammer, S. Hemmati, M. Dickinson, P. M. Challis, S. Wolff, K. I. Clubb, A. V. Filippenko, H. Nayyeri, V. U, D. C. Koo, S. M. Faber, D. Kocevski, L. Bradley and

- D. Coe, “Type Ia Supernova Distances at Redshift > 1.5 from the Hubble Space Telescope Multi-cycle Treasury Programs: The Early Expansion Rate,” *Astrophys. J.* **853** (2018) no.2, 126 [arXiv:1710.00844 [astro-ph.CO]].
- [20] S. Alam *et al.* [BOSS], “The clustering of galaxies in the completed SDSS-III Baryon Oscillation Spectroscopic Survey: cosmological analysis of the DR12 galaxy sample,” *Mon. Not. Roy. Astron. Soc.* **470** (2017) no.3, 2617-2652 [arXiv:1607.03155 [astro-ph.CO]].
- [21] H. Gil-Marín, J. Guy, P. Zarrouk, E. Burtin, C. H. Chuang, W. J. Percival, A. J. Ross, R. Ruggeri, R. Tojerio, G. B. Zhao, Y. Wang, J. Bautista, J. Hou, A. G. Sánchez, I. Pâris, F. Baumgarten, J. R. Brownstein, K. S. Dawson, S. Eftekharzadeh, V. González-Pérez, S. Habib, K. Heitmann, A. D. Myers, G. Rossi, D. P. Schneider, J. L. Tinker and C. Zhao, “The clustering of the SDSS-IV extended Baryon Oscillation Spectroscopic Survey DR14 quasar sample: structure growth rate measurement from the anisotropic quasar power spectrum in the redshift range $0.8 < z < 2.2$,” *Mon. Not. Roy. Astron. Soc.* **477** (2018) no.2, 1604-1638 [arXiv:1801.02689 [astro-ph.CO]].
- [22] R. Ruggeri, W. J. Percival, H. Gil-Marín, F. Beutler, E. M. Mueller, F. Zhu, N. Padmanabhan, G. B. Zhao, P. Zarrouk and A. G. Sánchez, *et al.* “The clustering of the SDSS-IV extended Baryon Oscillation Spectroscopic Survey DR14 quasar sample: measuring the evolution of the growth rate using redshift space distortions between redshift 0.8 and 2.2,” *Mon. Not. Roy. Astron. Soc.* **483** (2019) no.3, 3878-3887 [arXiv:1801.02891 [astro-ph.CO]].
- [23] V. de Sainte Agathe, C. Balland, H. du Mas des Bourboux, N. G. Busca, M. Blomqvist, J. Guy, J. Rich, A. Font-Ribera, M. M. Pieri, J. E. Bautista, K. Dawson, J. M. Le Goff, A. de la Macorra, N. Palanque-Delabrouille, W. J. Percival, I. Pérez-Ràfols, D. P. Schneider, A. Slosar and C. Yèche, “Baryon acoustic oscillations at $z = 2.34$ from the correlations of $\text{Ly}\alpha$ absorption in eBOSS DR14,” *Astron. Astrophys.* **629** (2019), A85 [arXiv:1904.03400 [astro-ph.CO]].

- [24] K. Dutta, A. Roy, Ruchika, A. A. Sen and M. Sheikh-Jabbari, “Cosmology with low-redshift observations: No signal for new physics,” *Phys. Rev. D* **100** (2019) no.10, 103501 [arXiv:1908.07267 [astro-ph.CO]].
- [25] A.G. Polnarev, “Polarization and anisotropy induced in the microwave background by cosmological gravitational waves,” *Sov. Astron.* **29** (1985) 607.
- [26] M. M. Basko and A. G. Polnarev, “Polarization and anisotropy of the relict radiation in an anisotropic universe,” *Mon. Not. Roy. Astron. Soc.* **191** (2080) 207.
- [27] D. D. Harari and M. Zaldarriaga, “Polarization of the microwave background in inflationary cosmology,” *Phys. Lett. B* **319** (1993), 96-103 [arXiv:astro-ph/9311024 [astro-ph]].
- [28] M. Zaldarriaga and D. D. Harari, “Analytic approach to the polarization of the cosmic microwave background in flat and open universes,” *Phys. Rev. D* **52** (1995) 3276 [astro-ph/9504085].
- [29] K. L. Ng and K. W. Ng, “Large scale polarization of the cosmic microwave background radiation,” *Phys. Rev. D* **51** (1995), 364-368 [arXiv:astro-ph/9305001 [astro-ph]].
- [30] K. L. Ng and K. W. Ng, “Large-angle Polarization of the Cosmic Microwave Background Radiation and Reionization,” *Astrophys. J.* **456** (1996), 413-421 [arXiv:astro-ph/9412097 [astro-ph]].
- [31] M. Kamionkowski, A. Kosowsky and A. Stebbins, “Statistics of cosmic microwave background polarization,” *Phys. Rev. D* **55** (1997), 7368-7388 [arXiv:astro-ph/9611125 [astro-ph]].
- [32] J. R. Pritchard and M. Kamionkowski, “Cosmic microwave background fluctuations from gravitational waves: An Analytic approach,” *Annals Phys.* **318** (2005), 2-36 [arXiv:astro-ph/0412581 [astro-ph]].
- [33] W. Zhao and Y. Zhang, “Analytic approach to the CMB polarizations generated by relic gravitational waves,” *Phys. Rev. D* **74** (2006) 083006 [astro-ph/0508345].

- [34] N. Kitazawa, “On CMB B-modes and the Onset of Inflation,” JCAP **1908** (2019) 005 [arXiv:1906.07440 [astro-ph.CO]].
- [35] S. Chandrasekhar, “Radiative Transfer, ” New York: Dover Publications, Inc. 1960.
- [36] P. Cabella and M. Kamionkowski, “Theory of cosmic microwave background polarization,” astro-ph/0403392.
- [37] J. E. Gunn and B. A. Peterson, “On the Density of Neutral Hydrogen in Intergalactic Space,” Astrophys. J. **142** (1965) 1633.